Computational study of the propagation of the longitudinal velocity in a polymer melt contained within a cylinder using a scale-bridging method

Subhranil De

Department of Physics, Indiana University Southeast, New Albany, Indiana 47150, USA

(Received 20 November 2012; revised manuscript received 21 May 2013; published 20 November 2013)

The "constitutive equation"–free scale-bridging method connecting nonequilibrium molecular dynamics and continuum fluid mechanics, that had hitherto been applied only to a parallel-plates geometry, is extended to study the flow of a polymer melt in a cylindrical pipe subject to a velocity in the direction parallel to the cylinder's axis. The system, initially at rest, is given a velocity at the cylinder's surface, and the evolution of the velocity profile within the fluid is studied, along with the time taken for the velocity to propagate toward the cylinder's axis. The said time of propagation is found to increase with the boundary velocity—a fact in contrast with the case of a Newtonian fluid for which the time of propagation is expected to be independent of the boundary velocity. For a fixed value of the boundary velocity, the propagation time is found to increase with the cylinder radius according to a power law with an exponent that is smaller than the corresponding exponent for a Newtonian fluid. For the lower values of the boundary velocity and the lower values of the radius studied, a velocity overshoot is observed at the cylinder's axis—a manifestation of elastic behavior of the fluid.

DOI: 10.1103/PhysRevE.88.052311 PACS number(s): 83.10.Rs, 83.80.Sg, 83.60.Df, 47.11.−j

I. INTRODUCTION

Viscoelastic fluids are fluids that possess both viscous and elastic properties. Examples of viscoelastic fluids include polymeric liquids, colloids, and metals at very high temperatures. Many biological fluids including blood are viscoelastic as well. These fluids exhibit complex flow behaviors that are connected to microscale dynamics. Investigation of these peculiar flow behaviors has a wide range of applications in various scientific and technological fields, including biological science, chemical engineering, materials science, and mechanical engineering. Traditionally, computer simulations of flow properties of fluids resort to either continuum fluid mechanics or molecular dynamics (MD). Continuum fluid mechanics relies on a "constitutive relationship" between stress and flow details (e.g., flow state and flow history), which in general, for a viscoelastic fluid, is hard to establish for an arbitrary flow. On the other hand, since MD resorts to an atomistic model, with full-fledged MD simulations the computational requirements scale nearly linearly with system size, rendering the method practically inapplicable for flow at large length scales. Over the years several hybrid methods [1–5] have been developed that connect different regions of the fluid system where part of the system is simulated using MD and the rest using continuum fluid mechanics. These methods prove to be an excellent tool in investigating flow patterns in small molecule fluids where a "constitutive equation"–based continuum fluid mechanics (e.g., the Navier-Stokes equations for a Lennard-Jones fluid) correctly describes the flow of the fluid in one region but in other regions that have a large gradient of the velocity or the density field an MD simulation is more appropriate. Rheology of a polymer melt is characterized by nonlinear viscoelasticity [6,7] and memory effects [8], once again making the construction of a constitutive relationship difficult, which resulted in a considerable amount of effort put forth during recent years in developing multiscale methods to simulate the flow behavior of polymer melts. The hybrid methods mentioned previously are challenging to apply to viscoelastic fluids like a polymer melt, since the continuum part of the simulation relies on a constitutive equation. In a previous paper [9], we proposed a constitutive equation–free scale-bridging method that involves the simulation of only parts of the system using nonequilibrium molecular dynamics (NEMD) simulations, where the different parts only occasionally exchange information through a continuum fluid mechanics scheme. The said method was applied to the bead-spring model for a polymer melt embedded in a parallel-plates geometry subject to antisymmetric velocity boundary conditions, and its validity was checked by comparing the results with those obtained through a full-fledged NEMD simulation of the system. A variant of the constitutive equation–free scale-bridging method was used by Yasuda and Yamamoto in a series of papers [10–12] that involved the study of flow in polymeric fluids confined in a parallel-plates geometry. Ilg *et al.* [13–15] have developed thermodynamically guided, "time-scale bridging" multiscale simulation methods which they successfully applied to flow of unentangled polymer melts.

Although initially the main goal of the scale-bridging method was to save computation time by simulating only parts of the system, it turns out that the utility of the method goes far beyond that original goal. To be specific, the method can be applied to incompressible fluids in arbitrary geometries as long as at every point within the system the fluid locally undergoes a pure shear (i.e., no elongation or compression). If the geometry in question is not a periodic structure, in order to perform a full-fledged MD simulation one needs to incorporate an atomistic model of a boundary wall [4,5,7] as well, which presents an additional component of complexity to the simulation scheme. In our scale-bridging scheme, the MD simulation boxes representing the different parts of the fluid system are subject to the Lees-Edwards periodic boundary condition, thereby precluding the need of modeling a wall enclosing the whole geometry. In a situation as such, our scale-bridging method is deemed a natural choice for simulating flow in the system if one chooses to start from an

atomistic model of the fluid. Moreover, for a system possessing some symmetry, one could utilize that symmetry to achieve an even greater computational gain through the scale-bridging scheme. In the present work, we show how to extend the scale-bridging method to a fluid embedded in a cylindrical geometry and subject to a boundary velocity on the cylinder's surface in the direction parallel to the cylinder's axis. Since the said system possesses cylindrical (azimuthal) symmetry, the effective computational gain achieved through the use of the scale-bridging method is one order of magnitude higher compared to the situation where the method is used for a parallel-plates geometry.

Flow of viscoelastic fluids embedded in a cylindrical geometry is a common scenario in both biology and engineering and is hence extensively studied, and its examples include blood flowing through veins and arteries [16,17], ultrafiltration [18], and protein and DNA transport through membrane channels [19]. In the present work we apply the extended scale-bridging method to the same model for a polymer melt that we used in the previous work [9], and study how a sudden change of the boundary velocity from zero to a constant finite value propagates toward the axis of the cylinder. We study how the propagation time varies with the value of the boundary velocity and the system size, and compare the results with those expected for a Newtonian fluid embedded in the same geometry and subject to the same velocity boundary condition. The following sections are organized as follows: Section II gives a brief overview of different constitutive equations for viscoelastic fluids along with a brief review of the constitutive equation–free scale-bridging method applied to a parallel-plates geometry. Section III discusses the condition under which the method can be extended to a different geometry, and then gives details of how the method is extended to a cylindrical geometry with a boundary velocity parallel to the axis—the focus of this paper. Section IV gives details of what we study in this paper as an example boundary condition and presents simulation results. Section V discusses the dependence of the simulation results on the macro time step and the system resolution chosen, while Sec. VI discusses the computational gain achieved in the presence of the cylindrical symmetry. In Sec. VII we conclude with a summary and discussions.

II. CONSTITUTIVE EQUATIONS FOR VISCOELASTIC FLUIDS: OVERVIEW OF THE CONSTITUTIVE EQUATION–FREE SCALE-BRIDGING METHOD IN A PARALLEL-PLATES GEOMETRY

In the previous work [9] we considered one-dimensional flow, i.e., where the macroscopic velocity $\vec{v}$ has only one non-vanishing component v_x, which in turn is a function of the y coordinate only. The continuum equation connecting the change in velocity and the stress tensor in this situation is given by

$$\rho \frac{\partial v_x}{\partial t} = \frac{\partial \sigma_{xy}}{\partial y}, \tag{1}$$

where ρ is the density of the fluid.

For one-dimensional flow, the constitutive equation that connects the shear stress σ_{xy} and the shear rate $\frac{\partial v_x}{\partial y}$ for a Newtonian fluid [20] is

$$\sigma_{xy} = \mu \frac{\partial v_x}{\partial y}, \tag{2}$$

where μ is the constant viscosity of the fluid. Putting the above relation in (1), one obtains the Navier-Stokes equation for one-dimensional flow [20]:

$$\rho \frac{\partial v_x}{\partial t} = \mu \left(\frac{\partial^2 v_x}{\partial y^2} \right). \tag{3}$$

The most straightforward extension of Eq. (2) to a non-Newtonian fluid is to allow the viscosity to be dependent on the shear rate, the simplest such dependence being a power law [21] of the form

$$\mu \propto \left| \frac{\partial v_x}{\partial y} \right|^n. \tag{4}$$

If $n > 0$, we have a dilatant or shear-thickening fluid. If $n < 0$, then fluid is pseudoplastic or shear thinning.

The first step toward extending Eq. (2) to a viscoelastic fluid is the well-known Maxwell model [22], which contains an extra term on the left-hand side of the equation as follows:

$$\sigma_{xy} + \lambda \frac{\partial \sigma_{xy}}{\partial t} = \mu \frac{\partial v_x}{\partial y}, \tag{5}$$

where λ is the relaxation time. For a steady state, the shear stress σ_{xy} is a constant, and hence the above equation yields Eq. (2) for a Newtonian fluid. On the other hand, for a sudden change in the shear stress, the term $\lambda \frac{\partial \sigma_{xy}}{\partial t}$ on the left-hand side of Eq. (5) dominates, and by integrating (5) with respect to time one obtains $\lambda \sigma_{xy} = \mu \gamma$, which is the equation for an elastic solid with a shear modulus of μ/λ, γ being the net shear. A further extension of the Maxwell model is the constitutive relation proposed by Jeffreys [23],

$$\sigma_{xy} + \lambda \frac{\partial \sigma_{xy}}{\partial t} = \mu \frac{\partial v_x}{\partial y} + \eta \frac{\partial}{\partial t} \left(\frac{\partial v_x}{\partial y} \right), \tag{6}$$

η being a constant. This equation is capable of reproducing the delayed elastic motion for a sudden change in the shear stress. Further generalizations to models with multiple relaxation times have been proposed as well [24–27]. Another model for viscoelastic fluids is obtained through the generalization of the Maxwell model along a different route that involves fractional time derivatives of the shear stress and the shear rate [28,29],

$$\sigma_{xy} + \lambda^a \frac{\partial^a \sigma_{xy}}{\partial t^a} = \mu \lambda^{b-1} \frac{\partial^{b-1}}{\partial t^{b-1}} \left(\frac{\partial v_x}{\partial y} \right). \tag{7}$$

In the above equation describing the fractional Maxwell model, the constants a and b are fractional calculus parameters satisfying $0 \leqslant a \leqslant b \leqslant 1$, and once again λ and μ are the relaxation time and the viscosity, respectively. While $a = b = 1$ yields the regular Maxwell model, $a = 0$ and $b = 1$ yields the regular Newtonian fluid.

When the flow of a viscoelastic fluid is computed using a constitutive relation, a suitable model must be chosen that is appropriate to the physical properties of the system (e.g., the identity of the fluid, temperature, boundary conditions in terms of velocity or stress), and the values of all the different parameters in the model must be specified in advance.

However, no comprehensive set of methods exists that allows one to systematically choose the most appropriate constitutive equation and the values of the parameters for any given viscoelastic fluid and any set of system properties. Within our previous scale-bridging method, as briefly described below, the shear stresses at different parts of the fluid are directly calculated through nonequilibrium MD simulations starting from an atomistic force model, thereby precluding the need of a constitutive equation on the continuum level, which gives the method a distinct advantage over other methods that rely on a constitutive equation.

As part of the scale-bridging scheme, the system is divided into several slices of equal thickness Δy, and each slice is represented by a MD simulation box. Each such simulation box at a given time is subject to the shear rate $\frac{\partial v_x}{\partial y}$ at the middle of the slice, and is accordingly subject to Lees-Edwards periodic boundary conditions in the y direction, while regular boundary conditions are applied in the x and the z direction, respectively. Independent MD simulations are done in the simulation boxes through a coarse time interval Δt, and the shear stress σ_{xy} is calculated in each box using the virial expression

$$\sigma_{ij} = (1/V)\left[-nk_BT\delta_{ij} + \sum_{\alpha}\left\{r_\alpha^{-1}U'_\alpha(r_\alpha)r_{\alpha i}r_{\alpha j}\right\}\right], \tag{8}$$

where V is the volume of the MD simulation box, $U_\alpha(r_\alpha)$ the net potential between the two particles belonging to the particle pair labeled by α, and r_α the distance between the two particles in the pair. $U'_\alpha(r_\alpha)$ is the derivative of the potential with respect to the distance r_α. The shear stress σ_{xy} calculated using (8) in turn represents the shear stress at the corresponding slice. At the end of the coarse time interval Δt the velocities at all the interfaces between successive slices are updated using a finite difference form of (1). This updates the shear rate $\frac{\partial v_x}{\partial y}$ of each slice, and hence that in the corresponding MD simulation box as well. For the next set of MD simulations corresponding to the next Δt, for each simulation box the starting configurations of the constituent particles is the same as the configuration at the end of the previous Δt, which ensures that memory effects are properly captured. At the end of this next Δt, velocities are updated once again, and so forth, the process repeating itself through the duration of the simulation. The fact that the linear dimension of the MD simulation box may be taken to be much smaller than the thickness Δy of each slice leads to a prospective saving of computation time, since that way we effectively simulate only parts of the whole system. Denoting the length of the MD simulation box by L, we can define the scale factor f as $f = \Delta y/L$, which is an approximate measure of the ratio of the computation time required to simulate all parts of the system to the computation time required to simulate only parts of the system through the scale-bridging scheme. In principle, though, f can be taken to be smaller than 1 as well, in case the whole system is small enough and we are interested in finer resolutions of the continuum velocity profiles obtained.

III. EXTENSION OF THE SCALE-BRIDGING METHOD TO A DIFFERENT GEOMETRY

In our scale-bridging method applied to a parallel-plates geometry, each MD simulation box that represents a part of the system is subject to Lees-Edwards periodic boundary conditions which effectively impose a finite shear rate across the simulation box. Since both the volume of the simulation box and the number of particles within the box are fixed, the density of the fluid is fixed as well, i.e., the fluid is incompressible so that $\vec{\nabla}\cdot\vec{v} = 0$ holds for the continuum velocity at any point in the fluid. Hence, we could extend our scale-bridging method to general geometries involving flow of an incompressible fluid where each part of the system undergoes a pure shear, since in that case every part could still be represented by a MD simulation box subject to the appropriate Lees-Edwards periodic boundary conditions. This excludes situations involving elongation or compression of any parts of the system. This implies that for two-dimensional flow (we take the velocity $\vec{v}$ to depend on x and y, but not z) the conditions that

$$\begin{aligned}\frac{\partial v_x}{\partial x} &= 0\\ \frac{\partial v_y}{\partial y} &= 0\end{aligned} \tag{9}$$

must be met. The general relation connecting the change in a velocity component v_i at any point within the fluid to the stress components is given by

$$\rho\frac{\partial v_i}{\partial t} = \frac{\partial \sigma_{ij}}{\partial r_j}, \tag{10}$$

where Einstein's summation convention is implied.

A. The scale-bridging method for the present cylindrical geometry

In the present work we consider a situation involving an incompressible fluid embedded in a cylinder of radius R with the surface of the cylinder moving parallel to the axis of the cylinder (which we call the z axis, following convention), as shown in Fig. 1. The system is infinite in extent in both directions parallel to the z axis.

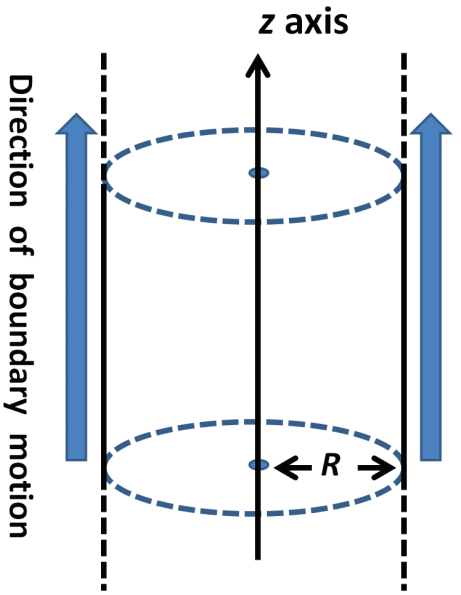

FIG. 1. (Color online) The geometry of the present problem and the direction of the velocity at the surface.

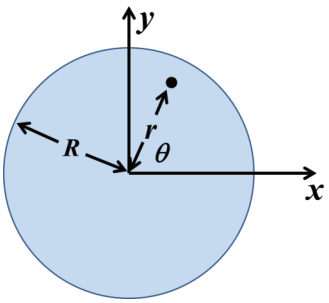

FIG. 2. (Color online) A cross section of the cylindrical geometry.

The radial and the azimuthal coordinates are denoted by r and θ, respectively, as shown in the perpendicular cross section of the system sketched in Fig. 2. We take the fluid to be initially at rest and give the surface of the cylinder a sudden constant velocity in the z direction, so that the velocity boundary condition is

$$\begin{aligned} v_z(r = R, t \leqslant 0) &= 0 \\ v_z(r = R, t > 0) &= v_0. \end{aligned} \tag{11}$$

We are interested in studying the propagation of the velocity through the fluid toward the cylinder's axis. In this case the only nonvanishing component of the velocity of the fluid will be the z component v_z, which will be independent of both z and θ and will be a function of r and time t only. The continuum equation connecting the change in v_z and the stress tensor in this situation is given by

$$\rho \frac{\partial v_z}{\partial t} = \frac{1}{r} \frac{\partial (r \sigma_{zr})}{\partial r}. \tag{12}$$

For a Newtonian fluid with a constant viscosity μ, by using $\sigma_{zr} = \mu \frac{\partial v_z}{\partial r}$, we retrieve from (12) the Navier-Stokes form for the change in v_z for the geometry and boundary conditions at hand, namely,

$$\rho \frac{\partial v_z}{\partial t} = \mu \left(\frac{\partial^2 v_z}{\partial r^2} + \frac{1}{r} \frac{\partial v_z}{\partial r} \right). \tag{13}$$

Since in our present problem we focus on our viscoelastic polymeric fluid, Eq. (13) is not expected to hold. In order to apply our extended scale-bridging method to the present problem, we decompose our cylindrical geometry into N coaxial cylindrical shells each of thickness Δr. The cross section of the scheme is shown in Fig. 3.

As shown, without losing generality we take the grid points on the positive x axis and the continuum velocity (which is parallel to the z axis in this case) is updated with time at each grid point. A gauss point containing an MD simulation box is taken midway between every two successive grid points. Since the gauss points are on the positive x axis, the shear stress σ_{zr} at the gauss points is given by $\sigma_{zr} = \sigma_{zx}$.

Now, there are $(N + 1)$ grid points in total. For the grid point on the cylinder surface at a distance R from the center (the one farthest to the right in Fig. 3), the continuum velocity is provided through the velocity boundary condition (11). For each of the rest of the grid points except the one at the very center, we can arrive at a scheme to update its continuum velocity v_z using Newton's second law. For the grid point under consideration, let us take its distance from

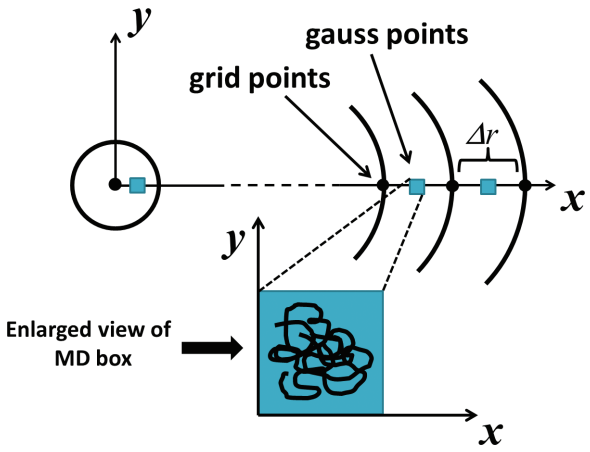

FIG. 3. (Color online) Schematic of the scale-bridging scheme applied to the present cylindrical geometry. The black dots are the grid points, and each small cube midway between two successive grid points is a gauss point where a cubic MD simulation box is taken as a representative of the system between the two grid points. The continuum velocity is in the z direction, the positive z direction being perpendicular to the plane of the page and out of the page.

the center to be r. We consider an annular cylinder of fluid of height h having an inner radius of $r_i = r - (\Delta r/2)$ and an outer radius of $r_0 = r + (\Delta r/2)$, thus containing one gauss point on the inner surface and the outer surface each. The net force on this annular cylinder in the positive z direction will be $F = 2\pi h[r_o(\sigma_{zr})_o - r_i(\sigma_{zr})_i]$. The volume of the same annular fluid cylinder is $\pi[r_o^2 - r_i^2]h$, and hence the mass is $\pi[r_o^2 - r_i^2]h\rho$. Equating the expression of the force to the mass times the acceleration $\frac{\partial v_z}{\partial t}$ of the annular cylinder, and writing that acceleration in finite difference form we get, after slight rearranging,

$$\frac{\Delta v_z}{\Delta t} = \frac{1}{\rho r} \left[\frac{r_o(\sigma_{zr})_o - r_i(\sigma_{zr})_i}{\Delta r} \right]. \tag{14}$$

It is worth noting that (14) is essentially the finite difference form of (12). In terms of the stresses calculated at the gauss points in Fig. 3, we can rewrite (14) as

$$\Delta v_z = \frac{1}{\rho r} \left[\frac{r_o(\sigma_{zx})_o - r_i(\sigma_{zx})_i}{\Delta r} \right] \Delta t, \tag{15}$$

which is the relation we use to update the velocity v_z at the grid point.

Updating the velocity at the center of the circle (i.e., at the cylinder axis) has to be treated as a special case. This is because unlike all the other grid points the center is a point that is not situated between two gauss points. We consider the innermost fluid cylinder of height h and radius $(\Delta r/2)$, containing on its surface the gauss point farthest to the left in Fig. 3. The entire surface of this cylinder is exposed to a shear stress that is equal to $(\sigma_{zr})_o$—the same as the shear stress $(\sigma_{zx})_o$ at the said gauss point. The net force on this cylinder is $F = 2\pi h[(\Delta r/2)(\sigma_{zr})_o]$, and the net mass is $\pi(\Delta r/2)^2 h\rho$. As before, Using Newton's second law to arrive at an expression of the acceleration of the innermost fluid cylinder and then taking its finite difference form, we write, after simplifying, the equation to update the velocity v_z (which is taken to be the velocity at the cylinder axis as well) of the central cylinder

under consideration,

$$\Delta v_z = \frac{4(\sigma_{zx})_o}{\rho(\Delta r)}\Delta t. \tag{16}$$

For every macro time step Δt (given by $\Delta t = 100\delta t$, δt being the length of one MD time step), nonequilibrium MD simulations are done in each MD simulation box situated between two successive grid points, with each such box subject to a shear rate $\frac{\partial v_z}{\partial x}$ calculated from the finite difference expression

$$\frac{\partial v_z}{\partial x} \approx \frac{(v_z)_o - (v_z)_i}{\Delta r}, \tag{17}$$

where now the subscript o refers to the grid point on the right, and the subscript i refers to the grid point on the left. Accordingly, Lees-Edwards periodic boundary conditions are imposed on each MD simulation box along the x direction, and regular periodic boundary conditions are imposed in both the y and z directions. At the end of the coarse time step Δt the grid velocities are updated using (15) and (16), which updates the shear rates imposed on the different gauss points using (17), and a new set of MD simulations are started for the next coarse step Δt, and the process repeats. At the beginning of every coarse time step Δt, in any MD simulations box the configuration of polymer chains is taken to be the same as that obtained at the end of the previous Δt, which ensures that memory effects are properly captured. Once again, if the length of the MD simulation box is denoted by L, for the present geometry we can define the scale factor f as $f = \Delta r/L$. In the present situation, though, because of the cylindrical symmetry of the system, the effective computational gain is much larger compared to the parallel-plates case. Details of the computational gain are discussed in Sec. VI.

At this point, it is worth discussing the singularity of the partial differential equation (12) at $r = 0$. The said equation has an r in the denominator on the right-hand side and hence $\partial v_z/\partial t$ becomes singular at $r = 0$. Incidentally, this singularity is a "removable singularity." Equation (12) can be rewritten as

$$\rho\frac{\partial v_z}{\partial t} = \frac{\partial \sigma_{zr}}{\partial r} + \frac{\sigma_{zr}}{r}. \tag{18}$$

If the shear field is to be continuous everywhere, then the cylindrical symmetry implies that at the axis, $(\partial v_z/\partial r) = 0$, which in turn implies that right at the axis the shear rate and hence the shear stress will be zero at all times.

Hence, as $r \to 0$, the shear stress $\sigma_{zr} \to 0$ as well, in such a way that the limiting value of $\partial v_z/\partial t$ as expressed through (18) is actually finite as $r \to 0$. Since we only use a finite difference scheme where the innermost MD box is taken at the midpoint of the innermost radial line segment, we are not supposed to run into any problems arising due to the singularity of Eq. (12) at the cylinder axis.

B. The atomistic polymer melt model and details of the NEMD simulation

The model for the polymer melt along with the MD simulation details of the present work are taken to be the same as those in the previous work [9] applied to the parallel-plates geometry. The model is the standard bead-spring model, with each polymer chain consisting of 120 beads, every two adjacent beads being connected through a finitely extensible nonlinear elastic (FENE) spring described by the potential $U_{\text{FENE}} = -(kR_0^2/2)\ln[1-(r/R_0)^2]$. Additionally, every pair of beads within the system interacts through a shifted, purely repulsive Lennard-Jones potential $U_{LJ} = 4\varepsilon[(\sigma/r)^{12} - (\sigma/r)^6] + \varepsilon$ for $r < 2^{1/6}\sigma$ and $U_{LJ} = 0$ otherwise, where ε has units of energy and σ that of length. Each MD simulation box is a cube of length 14.1σ, containing 20 polymer chains, making the total number of beads in the box 2400. The system is taken at a constant temperature, the value of which in dimensionless units is taken to be $T^* = k_BT/\varepsilon = 1$. The integration time step for the MD is taken to be $\delta t = 0.0008\tau$, where the characteristic time τ is defined as $\tau = \sigma\sqrt{m/\varepsilon}$, m being the mass of a single bead. In turn, each coarse time step is taken to be $\Delta t = 100\delta t$. Thermostating is performed by rescaling the velocities of the beads at the end of every MD time step, assuming a linear velocity profile in accordance with the shear rate $\frac{\partial v_z}{\partial x}$ imposed on the box. The MD step is chosen to be small since the condition $\Delta t \gg \delta t$ should be met within our scale-bridging scheme, and we choose a small enough value of Δt as well to start with, in order to ascertain that it is small compared to the time scale of the velocity and shear-rate variations within the system.

IV. THE DETAILS OF THE PRESENT FLOW PROBLEM AND SIMULATION RESULTS

For the velocity boundary condition given in (11), we expect the continuum velocity at the axis of the cylinder to approach the surface velocity as time goes on, i.e., $\lim_{t\to\infty} v_z(r=0) = v_0$. A measure of the time taken for the velocity to propagate from the cylinder's surface to the axis is the half time t_0, defined as the time taken for the continuum velocity on the axis to become equal to half of the velocity v_0 at the cylinder surface. If the fluid were a Newtonian fluid, it follows from the form of (13) that t_0 would be independent of v_0, i.e., the time of propagation would be independent of the boundary velocity. At the same time, it also follows from (13) that for a Newtonian fluid the variation of t_0 with the radius R of the cylinder would be $t_0 \propto R^2$ (the proof is in the Appendix). With our polymer melt taken within the cylindrical geometry of the present problem, we wish to study the variation of the half time with both the boundary velocity and the cylinder radius and want to compare the results with those for a situation involving a Newtonian fluid.

A. Velocity profiles in the polymer melt for a sample system size and boundary velocity

From now on, all results for simulations done with a polymer melt are reported in dimensionless units, i.e., with distance reported with respect to σ and time reported with respect to τ, as defined in Sec. III B. The dimensionless units are denoted with an asterisk (*). In this section we present some results for the scale-bridging simulations done with $N = 25$ cylindrical shells and a scale factor of $f = 1.0$, making the radius of the cylinder to be $R^* = 352.5$. The greater the value of the surface velocity v_0, the smaller the statistical fluctuations in the velocity calculated relative to the average (continuum) velocity, and hence the less noisy is the velocity data. A natural

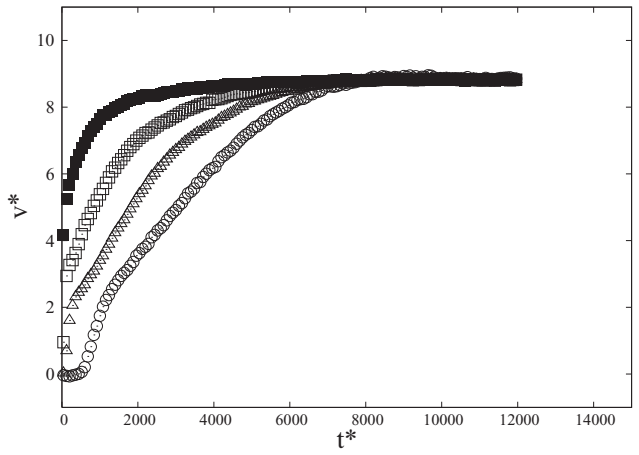

FIG. 4. The evolution of the normalized velocity at different values of the distance r^* from the axis of the cylinder for $R^* = 352.5$ and $v_0^* = 8.81$. The solid squares correspond to $r^* = 338.4$, the hollow squares to $r^* = 310.2$, the hollow triangles to $r^* = 267.9$, and the hollow circles to $r^* = 0$ (the axis).

velocity scale of the polymer melt can be estimated by dividing the root-mean-square value of the end-to-end chain distance in the system by the stress relaxation time. The value of the said end-to-end distance in dimensionless units for a chain size of 120 is of the order of 10^1 [30], and the value of the said stress relaxation time in dimensionless units is of the order of 10^4 [31], making the said natural velocity scale of the order of 10^{-3}. In order to obtain velocity data with low noise, we start with a high value of $v_0^* = 8.81$ for our first set of simulations.

Figure 4 shows the evolution of the velocity normalized with respect to the boundary velocity at different values of the distance from the cylinder's axis. A running average of the velocity is performed over every 1000 macro time steps to further smoothen out the noise. Among all the plots, the velocity at the axis trails behind the most, as expected. Figure 5 shows the plots of the velocity profiles, namely, the velocity plotted against the distance from the axis at different time instants.

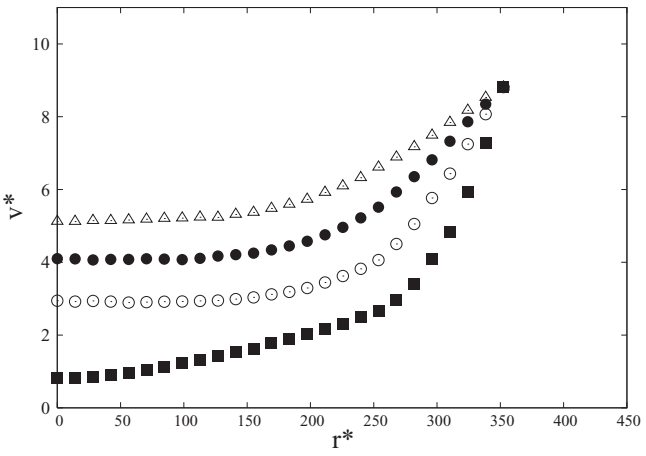

FIG. 5. Velocity profiles at different values of t^* for $R^* = 352.5$ and $v_0^* = 8.81$. The solid squares correspond to $t^* = 800.0$, the hollow circles to $t^* = 1600.0$, the solid circles to $t^* = 2400.0$, and the hollow triangles to $t^* = 3200.0$.

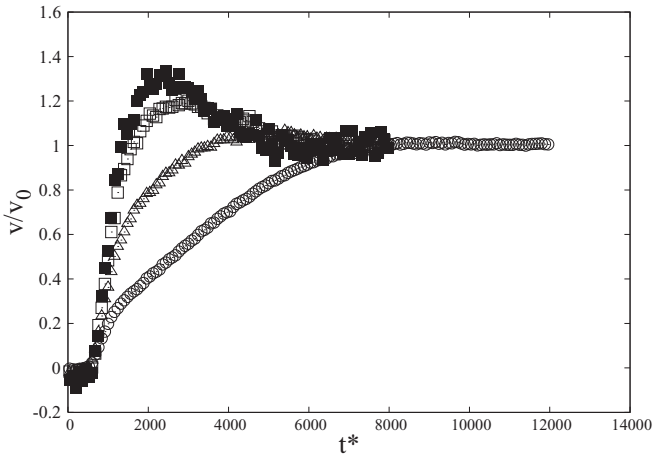

FIG. 6. The evolution of normalized velocity at the axis for different values of v_0^* for $R^* = 352.5$. The solid squares correspond to $v_0^* = 0.88$, the hollow squares to $v_0^* = 1.76$, the hollow triangles to $v_0^* = 3.53$, and the hollow circles to $v_0^* = 8.81$.

B. Dependence of the half time on boundary velocity for a fixed cylinder radius

In this section we report results for different values of the boundary velocity v_0^* for a fixed value of the radius, namely, $R^* = 352.5$. The different values of v_0^* used are $v_0^* = 0.88$, 1.76, 3.53, 5.29, 8.81, 12.33, and 17.62, respectively. Figure 6 shows the evolution of the normalized velocity v/v_0 at the axis with time for a few different values of v_0^*. There are two interesting observations to be made here. First, unlike the case with a Newtonian fluid, the velocity evolution profiles are clearly dependent on the boundary velocity. In particular, the greater the value of the boundary velocity is, the slower is the velocity evolution at the axis, i.e., the greater is the half time. Second, for the two lowest values of the boundary velocity (namely, $v_0^* = 0.88$ and 1.76), there is clearly a velocity overshoot, i.e., instead of asymptotically approaching the boundary velocity from below, the velocity at the axis reaches a maximum value that is greater than the boundary velocity and then approaches the value of the boundary velocity from above. This velocity overshoot is due to the viscoelastic nature of the polymer melt.

The half time t_0^* is calculated through linear interpolation between two successive data points that contain velocity values below and above the halfway mark, respectively, and the half time is plotted against v_0^* in Fig. 7. It clearly depicts the fact that the half time increases considerably with the value of the boundary velocity, e.g., the half time for $v_0^* = 17.62$ is about four times the half time for $v_0^* = 0.88$, a fact in sharp contrast with what would happen for a Newtonian fluid (for which the half time is expected to be independent of the boundary velocity). In regard to the finding that with the polymer melt the half time increases with the boundary velocity, we argue that it is caused by the fact that for larger boundary velocities the shear rates produced within the fluid are larger as well, leading to smaller effective viscosities consistent with the shear thinning behavior exhibited by polymer melts [32,33]. In turn, a smaller effective viscosity leads to a slower propagation of the change in velocity from one part of the system to another. It

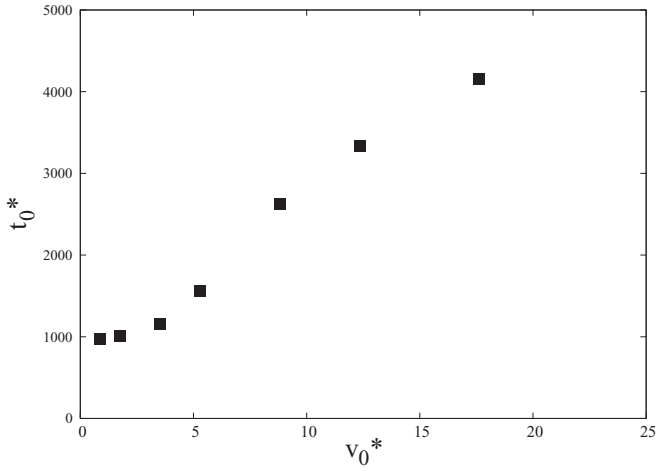

FIG. 7. The half time plotted against the boundary velocity for a cylinder radius value of $R^* = 352.5$. The half time increases with the boundary velocity, in contrast with Newtonian behavior where the half time is expected to be independent of the boundary velocity.

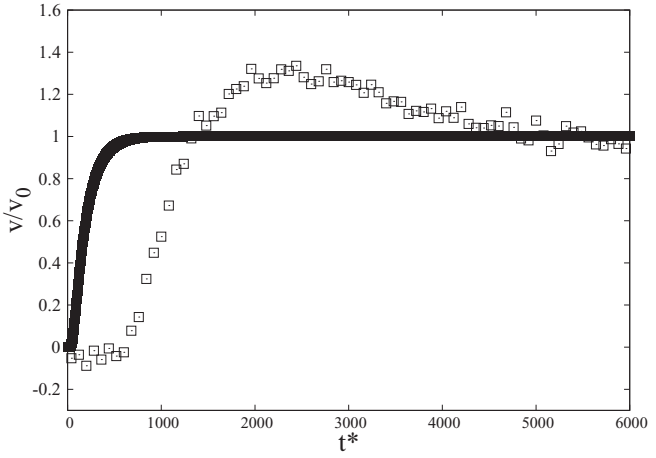

FIG. 8. Evolution of the normalized velocity at the cylinder axis for $R^* = 352.5$. The hollow squares correspond to the polymer melt system subject to a boundary velocity of $v_0^* = 0.88$. The solid line corresponds to a Newtonian fluid with a dimensionless viscosity of $\mu^* = 130$, which is equal to the zero-shear viscosity of the polymer melt.

is worth noting here though that the shear thinning in polymer melts refers to a reduction of a steady-state shear viscosity with increasing shear rates. In our present work which relates to a transient state, the velocity evolution within the system cannot be determined using the steady-state viscosities, since during the transient state the polymer melt exhibits memory effects, the reason that in this situation the scale-bridging method is needed to start with. Nevertheless, the finding that the half time increases with the boundary velocity is consistent with shear thinning.

We observe in Fig. 7 the pattern that the half time tends to reach a saturation value as v_0^* gets smaller. The limiting value of the half time for small v_0^* can be estimated by extrapolating the plot to the t_0^* axis. We perform a parabolic fit using the three lowest values of v_0^*, and obtain the said limiting value of the half time to be $t_0^* \approx 961$. This is a way around an attempt to calculate the limiting value of the half time by directly performing simulations at a very low v_0^*, since at some point for small enough values of v_0^* the fluctuations in v^* become comparable to the actual values of v^*, making a direct estimation of the velocity profiles and the half time difficult.

In order to study how well the velocity evolution profiles agree with the profile obtained using a corresponding Newtonian scheme, we resort to Eq. (13) for a Newtonian fluid. For the given polymer melt model, namely, FENE chains with a chain size of 120 at a dimensionless density of $\rho^* = 0.85$, the value of the dimensionless zero-shear viscosity is $\mu^* \approx 130$ [31]. Putting this value in the dimensionless form of (13), we numerically calculate the normalized velocity evolution at the axis for the value of the radius under consideration, namely, $R^* = 352.5$. This is plotted in Fig. 8, along with the normalized velocity evolution of our polymer melt for the $v_0^* = 0.88$ case. We observe that the evolutions of the normalized velocities hardly agree. Unlike the polymer melt, the Newtonian plot shows no overshoot, and the Newtonian half time of $t_0^* = 163$ is much smaller than the polymer melt half time of $t_0^* = 974$. This corroborates that the velocity evolution of the polymer melt cannot be calculated using the Navier-Stokes formalism for a Newtonian fluid. It is worth noting here that even in the limit $v_0^* \to 0$, the velocity evolution profile cannot be expected to be inferred using the Newtonian scheme. This is due to the fact that even for small values of shear rates involved, the polymer melt still possesses a long stress relaxation time, making it exhibit strong memory effects that play a role in its rheology. In contrast, a classical Newtonian fluid is essentially memory-free in the sense that the shear stress at any point only depends on the then shear rate.

C. Dependence of the half time on cylinder radius for a fixed boundary velocity

This section pertains to results for scale-bridging simulations done with still $N = 25$ cylindrical shells and a fixed value of the boundary velocity v_0^*, but for different values of the scale factor, namely, $f = 0.5$, 0.75, 1.0, 1.25, 1.5, 1.75, and 2.0, making the corresponding values of the cylinder radius to be $R^* = 176.3$, 264.4, 352.5, 440.6, 528.8, 616.9, and 705.0, respectively.

Figure 9 shows the time evolution of the velocity at the cylinder's axis normalized with respect to the boundary velocity $v_0^* = 1.76$ for different values of the cylinder radius. The time taken for the surface velocity to propagate to the cylinder axis increases with cylinder radius, as expected, thus leading to an increase in the half time. Another interesting observation is that there is a velocity overshoot at the axis, but the overshoot (relative to the boundary velocity) decreases with increasing cylinder radius.

For a Newtonian fluid the half time is expected to vary with cylinder radius as $t_0 \propto R^2$. In order to investigate if a similar power law behavior of the form $t_0 \propto R^\xi$ exists in the present polymer melt case, we make a log-log plot of the half time versus the cylinder radius, shown in Fig. 10. For $v_0^* = 1.76$, a straight line fit of the plot gives a value of the exponent to be $\xi = 1.47 \pm 0.01$, which is considerably smaller than the corresponding value of 2 for a Newtonian fluid. A similar scheme with simulation data for a higher value of the boundary

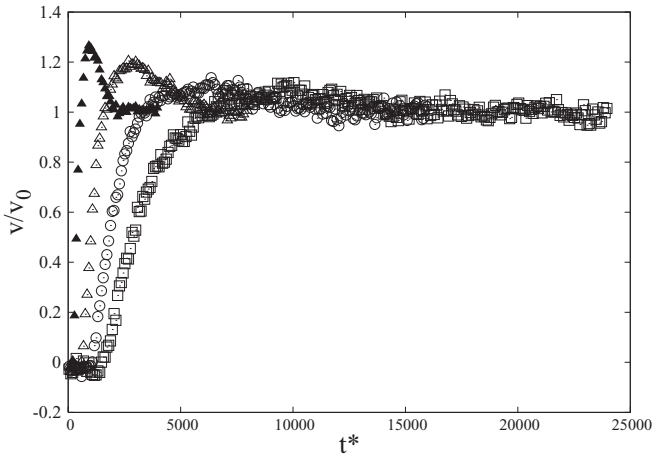

FIG. 9. The evolution of the normalized velocity at the cylinder axis for different values of the cylinder radius for $v_0^* = 1.76$. The filled triangles correspond to $R^* = 176.3$, the hollow triangles to $R^* = 352.5$, the hollow circles to $R^* = 528.8$, and the hollow squares to $R^* = 705.0$. The half time increases and the velocity overshoot decreases with cylinder radius.

velocity, namely, $v_0^* = 8.81$, yields a higher value of the exponent, $\xi = 1.84 \pm 0.04$, which is still smaller than the Newtonian value of 2. We have already observed that a lower boundary velocity leads to faster variations of velocities and shear rates within the polymer melt (thus leading to a smaller half time)—in other words, the said variations occur at a time scale that is even shorter compared to the long stress relaxation times of the fluid, leading to more pronounced memory effects. This is consistent with the fact that the scaling exponent obtained for a low v_0^* is even more deviated from the Newtonian exponent of 2.

It is worth mentioning here that in the regime of very low v_0^*, where the whole range of shear rates involved will be accordingly low as well, determining the velocity profiles requires enormous computational resources. For a situation like that, resorting to a computational method like the ones elaborated in Refs. [13–15] may be more appropriate.

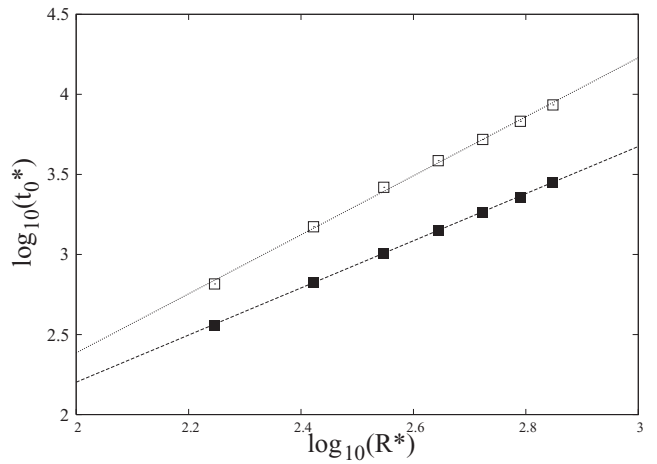

FIG. 10. Log-log plot of half time versus cylinder radius. The filled squares correspond to $v_0^* = 1.76$, yielding an exponent value of 1.47 ± 0.01, and the hollow squares correspond to $v_0^* = 8.81$, yielding an exponent value of 1.84 ± 0.04.

V. DEPENDENCE ON THE CHOICE OF THE MACRO TIME STEP AND THE SYSTEM RESOLUTION

A. The macro time step Δt

There remains a possibility that the macro time step Δt we used is too long in the sense that we might lose a substantial amount of information regarding the changing velocities and shear rates within the cylinder during each Δt. In order to verify that this is not true, we take the case of $f = 1.0$ ($R^* = 352.5$) and take the largest and the smallest boundary velocities, namely, $v_0^* = 17.62$ and $v_0^* = 0.88$, respectively, and run the scale-bridging simulation with a much shorter macro time step given by $\Delta t = 10\delta t$, which is ten times shorter than the default macro time step used. The results for the velocity evolution at the axis obtained with the two different time steps used are shown in Figs. 11(a) and 11(b), respectively. As manifest in the plots, for each value of the boundary velocity, the velocities obtained at the axis using the two different values of Δt agree within the statistical fluctuations.

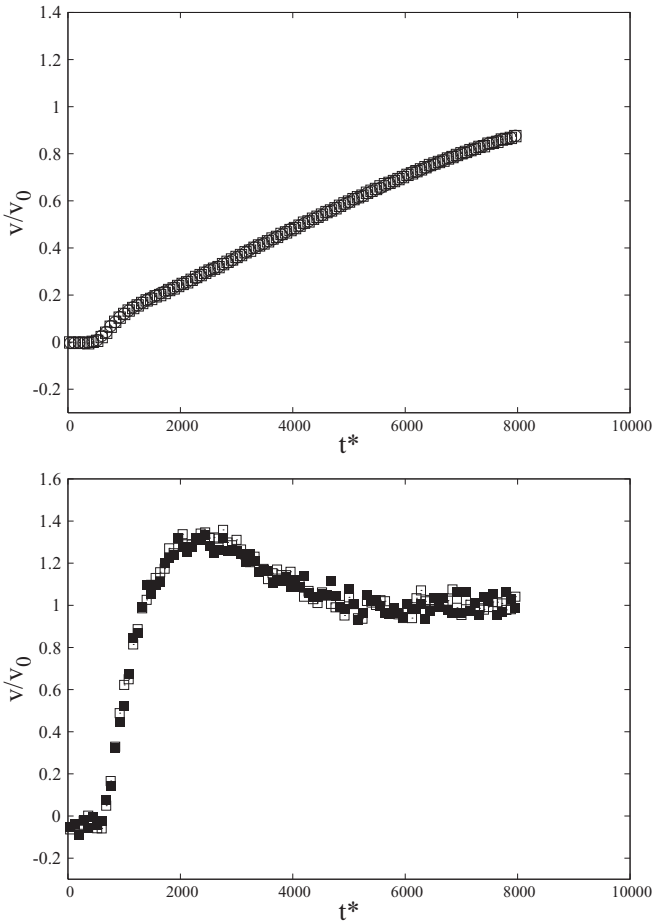

FIG. 11. (a) The evolution of the normalized velocity at the axis for $v_0^* = 17.62$ and $R^* = 352.5$ using two different values of Δt. The hollow squares correspond to $\Delta t = 100\delta t$ and the hollow circles correspond to $\Delta t = 10\delta t$. (b) The evolution of the normalized velocity at the axis for $v_0^* = 0.88$ and $R^* = 352.5$ using two different values of Δt. The solid squares correspond to $\Delta t = 100\delta t$ and the hollow squares correspond to $\Delta t = 10\delta t$.

B. The system resolution N

One obvious question with the data obtained through our scale-bridging scheme is whether the system resolution, namely, the number of slices N the cylinder is decomposed into, is large enough to produce reliable velocity profiles. In order to test this, we took two system realizations we have already simulated using $N = 25$, namely, (a) $v_0^* = 8.81$ and $R^* = 705.0$, and (b) $v_0^* = 8.81$ and $R^* = 352.5$. For each of the two cases (a) and (b), we now simulated the same system using a greater system resolution, namely, $N = 50$. The plots in Figs. 12(a) and 12(b) show that for each case the velocities calculated using the two different values of N at the same location within the cylinder agree very well within statistical fluctuations, thus leading us to believe that $N = 25$ is already a reliable degree of system resolution.

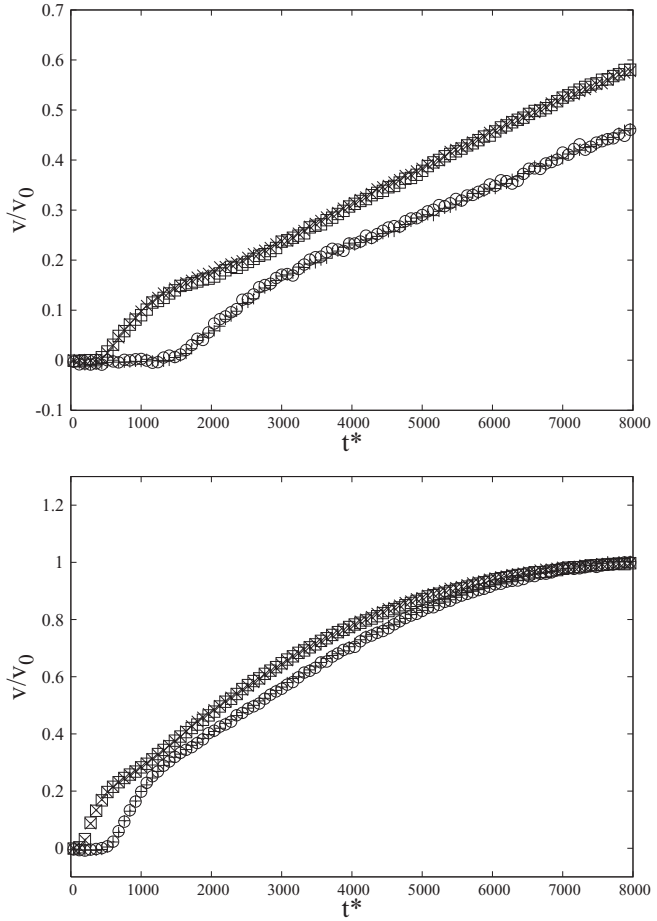

FIG. 12. (a) The evolution of the normalized velocity at the axis for $v_0^* = 8.81$ and $R^* = 705.0$ calculated using two values of the system resolution N. The hollow squares correspond to $r^* = 211.5$ using $N = 25$, the $\times$ symbols correspond to $r^* = 211.5$ using $N = 50$, the hollow circles correspond to $r^* = 0$ (the cylinder axis) using $N = 25$, and the $+$ symbols correspond to $r^* = 0$ using $N = 50$. (b) The evolution of the normalized velocity at the axis for $v_0^* = 8.81$ and $R^* = 352.5$ calculated using two values of the system resolution N. The hollow squares correspond to $r^* = 105.8$ using $N = 25$, the $\times$ symbols correspond to $r^* = 105.8$ using $N = 50$, the hollow circles correspond to $r^* = 0$ (the cylinder axis) using $N = 25$, and the $+$ symbols correspond to $r^* = 0$ using $N = 50$.

VI. COMPUTATIONAL GAIN FACTOR

We define the computational gain factor as the ratio of the computation time required to perform a full-fledged MD simulation of the whole system to the computation time required to simulate the same system using our scale-bridging scheme. Since the MD utilizes linked lists, the computation time required to directly simulate a part of the fluid is approximately proportional to its volume. Hence the computational gain factor can be taken to be the ratio of the fluid volume that needs to be simulated within a full-fledged MD scheme to the combined volume of all the MD simulation boxes used to simulate the system using the scale-bridging scheme. For a parallel-plates system, the computational gain factor is the same as the scale factor f defined before. However, the cylindrical symmetry for the system chosen in the present work lets us achieve a greater computational gain factor, which in this situation reduces to the ratio of the circular cross-sectional area of the cylinder to the combined cross-sectional area of all the MD boxes used for the scale-bridging simulation of the cylinder. Hence the computational gain factor g will be given by

$$g = \frac{\pi R^2}{NL^2}. \tag{19}$$

Since $\Delta r = R/N$ and $\Delta r/L = f$, relation (19) can be written as

$$g = \pi N f^2. \tag{20}$$

From the above relation we can calculate the computational gain factors achieved in the scale- bridging simulations reported in this paper. The largest computational gain factor was achieved for $N = 25$ and $f = 2.0$, the said largest value being about 314. The gain factor had its smallest value of about 20 for $N = 25$ and $f = 0.5$. As we can see, there is a considerable computational gain even when $f < 1$, due to the cylindrical symmetry of the system.

The above gain factors assume the same MD time step for a corresponding full-fledged MD simulation of the system. On the other hand, if we take into account the fact that the MD time step used in the scale-bridging simulations of the present work is about five times smaller than the standard MD time step used in FENE systems, even then the smallest and largest gain factor achieved turn out to be about 4 and 63, respectively.

VII. SUMMARY AND CONCLUSIONS

We extended the "constitutive equation"–free scale-bridging method previously applied to a parallel-plates geometry to study the flow of a viscoelastic polymer melt contained within a cylinder and subject to a boundary velocity directed parallel to the cylinder's axis. Similar to the original version of the method, the present version developed as well connects MD and continuum fluid mechanics while it takes into account the memory effect exhibited by the polymer melt. In addition, similar to the original version, the extended version as well is conducive to a saving of computation time through MD simulations of only parts of the system. We studied a situation where the velocity at the cylinder's surface is initially zero and then acquires a constant finite value, and calculated the half time defined as the time taken for the velocity at the axis to become half of the boundary

velocity. Thus the half time is a measure of the time taken for the change in velocity to propagate from the boundary to the axis. Using our scale-bridging method adopted for the cylindrical geometry, we performed two sets of simulations. In the first set, we studied the variation of the half time with the boundary velocity for a fixed cylinder radius. We observed that the half time increases significantly with the boundary velocity—manifesting that the propagation of the change in velocity from the boundary to the axis is slower for higher values of the boundary velocity. This is in contrast with the case with a Newtonian fluid, for which the propagation time is expected to be independent of the boundary velocity. The said behavior obtained with the polymer melt is consistent with an effective viscosity that is lower for a higher shear rate, in other words, shear thinning, a behavior polymer melts are known to manifest. It turns out that the normalized velocity evolution cannot be modeled with a Newtonian fluid with the appropriate viscosity, since the melt is fraught with strong memory effects due to its long stress relaxation time, which is true even for low shear-rate values.

In the second set of simulations we kept the value of the boundary velocity constant and studied the dependence of the half time on cylinder radius. This dependence is expected to be of the form $t_0 \propto R^2$ for a Newtonian fluid. Assuming a similar power-law dependence of the form $t_0 \propto R^{\xi}$ in the case of the polymer melt, we calculated the value of the exponent ξ, which turned out to be smaller than the Newtonian value of 2. The value of ξ turns out to be more deviated from the Newtonian value when the boundary velocity is smaller. We argue that this is due to the fact that for a lower boundary velocity the time scale of velocity and shear rate variations is even shorter compared to the long stress relaxation time of the melt, as observed, thus leading to even stronger memory effects. As a by-product of the simulations mentioned above, we observed a velocity overshoot behavior at the axis for low boundary velocities and small values of the cylinder radius. It is well known that when a polymer melt is first subject to a shear rate, it initially undergoes an overshoot in shear stress [8,34,35], a behavior arising from the elastic aspect of the viscoelasticity of the melt. The velocity overshoot we observed in our simulations is also a manifestation of elasticity of the polymer melt.

The situation chosen here is different from a steady-state situation, like the flow under a steady pressure gradient, where the scale-bridging method, although still useful, is deemed redundant. This is due to the fact that for any steady-state flow, a constitutive relationship between shear rates and corresponding steady shear viscosities (like the ones presented in the plots in Fig. 1(a) in Ref. [32] and Fig. 1(a) in Ref. [33]) can be directly used to determine the flow profiles. As a contrast, for a transient (unsteady) flow situation like the one chosen in the present work, a steady-state constitutive relationship is expected to fail since the flow properties are fraught with memory effects. To our knowledge, this is the first time a constitutive equation–free scale–bridging method connecting molecular dynamics and continuum fluid mechanics has been applied to any geometry other than the parallel-plates geometry. Since the method does not require a constitutive equation for the fluid, it can be used to study the flow of viscoelastic fluids for a wide range of geometries and boundary conditions given an atomistic model for the fluid. The situation studied in this paper, namely, longitudinal flow of a viscoelastic fluid embedded in a cylinder, is a common situation in both nature and engineering. For studying a transient (unsteady) flow problem in a cylindrical geometry starting from an atomistic model, the scale-bridging method is deemed a natural choice since a full-fledged MD simulation of the whole system necessitates the modeling of a wall enclosing the geometry as well. Moreover, the cylindrical symmetry of the system leads to an effective computation time gain that is much higher compared to the parallel-plates case. It is also worth noting that the scale-bridging method is not limited to only polymer melts composed of linear polymer chains. Starting with the appropriate atomistic model, our multiscale method can be used to study the flow behavior of other complex fluids [30] as well, including branched polymers, wormlike micelles, and colloidal fluids.

ACKNOWLEDGMENTS

The author gratefully acknowledges support through summer faculty fellowships from Indiana University Southeast. He would also like to thank the anonymous referees for all their valuable suggestions and constructive criticism.

APPENDIX

The velocity boundary condition given by Eq. (11) can be written as

$$v_z(r = R,t) = v_0 H(t), \tag{A1}$$

where $H(t)$ is the Heaviside step function. When the above boundary condition is applied to a cylindrical geometry of radius R containing a given Newtonian fluid, let us assume that the resulting velocity within the fluid is given by

$$v_z = f(r,t), \tag{A2}$$

which must solve the Navier-Stokes equation (13). Now, it can be shown through straightforward substitution that since (A2) is a solution to (13),

$$v_z = f(nr,n^2t) \tag{A3}$$

will be also a solution to (13) as well, where the number n is an arbitrary scale factor.

Hence we can infer that for the same fluid contained within a cylinder of a different radius R_n given by

$$R_n = nR, \tag{A4}$$

if we apply the velocity boundary condition

$$v_z(r = nR,t) = v_0 H(n^2t) \tag{A5}$$

to the cylinder's surface, then the resulting velocity within the fluid will be given by the relation (A3). Now the half time corresponds to the time evolution of the velocity at the axis, and for the cylinder of radius R_n, the said velocity will be given by $v_z(r = 0,t) = f(0,n^2t)$, and hence the half time t_n for the cylinder of radius R_n will be given by

$$t_n = n^2 t_0, \tag{A6}$$

where t_0 is the half time for the cylinder of radius R.

Now, for any constant $b > 0$, $H(bt) = H(t)$ [36]. Hence $H(n^2t) = H(t)$, and the velocity boundary condition at the surface of the cylinder of radius R_n, namely, relation (A5), is deemed the same as the one for the cylinder of radius R, namely, (A1). Hence using (A4) and (A6) we conclude that for the cylinder of radius R_n, if the cylinder surface is subject to a velocity given by $v_z(r = R_n,t) = v_0H(t)$, the corresponding half time will vary with the cylinder radius as

$$t_n/t_0 = R_n^2/R^2$$

or

$$t_n \propto R_n^2.$$

Hence proved.

[1] S. T. O'Connell and P. A. Thompson, Phys. Rev. E **52**, R5792 (1995).
[2] N. G. Hadjiconstantinou and A. T. Patera, Int. J. Mod. Phys. C **8**, 967 (1997).
[3] E. G. Flekkoy, G. Wagner, and J. Feder, Europhys. Lett. **52**, 271 (2000).
[4] X. B. Nie, S. Y. Chen, E. Weinan, and M. O. Robbins, J. Fluid. Mech. **500**, 55 (2004).
[5] X. Nie, S. Chen, and M. O. Robbins, Phys. Fluids **16**, 3579 (2004).
[6] M. Kroger and S. Hess, Physica A **195**, 336 (1993).
[7] R. Khare, J. de Pablo, and A. Yethiraj, J. Chem. Phys. **114**, 7593 (2001).
[8] U. Borgbjerg, J. de Pablo, and H. C. Ottinger, J. Chem. Phys. **101**, 7144 (1994).
[9] S. De, J. Fish, M. S. Shephard, P. Keblinski, and S. K. Kumar, Phys. Rev. E **74**, 030801(R) (2006).
[10] S. Yasuda and R. Yamamoto, Europhys. Lett. **86**, 18002 (2009).
[11] S. Yasuda and R. Yamamoto, Phys. Rev. E **81**, 036308 (2010).
[12] S. Yasuda and R. Yamamoto, Phys. Rev. E **84**, 031501 (2011).
[13] P. Ilg, Physica A **387**, 6484 (2008).
[14] P. Ilg, H. C. Öttinger, and M. Kröger, Phys. Rev. E **79**, 011802 (2009).
[15] P. Ilg and M. Kroger, J. Rheol. **55**, 69 (2011).
[16] G. A. Vlastos, Clin. Hemorheol. Microcirculation **19**, 177 (1998).
[17] H. A. Gonzalez Rojas, Med. Eng. Phys. **29**, 491 (2007).
[18] F. Jin and C. Wu, Phys. Rev. Lett. **96**, 237801 (2006).
[19] B. Alberts, A. Johnson, J. Lewis, M. Raff, K. Roberts, and P. Walter, *Molecular Biology of the Cell*, 4th ed. (Garland Science, New York, 2002).
[20] Robert A. Granger, *Fluid Mechanics* (Dover, New York, 1995).
[21] Susana Gabbanelli, German Drazer, and Joel Koplik, Phys. Rev. E **72**, 046312 (2005).
[22] J. C. Maxwell, Philos. Trans. R. Soc. London **157**, 49 (1867).
[23] H. Jeffreys, *The Earth* (Cambridge University Press, New York, 1976).
[24] R. B. Bird, R. C. Armstrong, and O. Hassager, *Dynamics of Polymeric Liquids* (Wiley, New York, 1987), Vol. 1.
[25] R. G. Larson, *Constitutive Equations for Polymer Melts and Solutions* (Butterworths, Boston, 1988).
[26] J. L. White and A. B. Metzner, J. Appl. Polym. Sci. **7**, 1867 (1963).
[27] G. Giesekus, J. Non-Newtonian Fluid Mech. **11**, 69 (1982).
[28] R. L. Bagley, J. Rheol. **30**, 133 (1986).
[29] T. Wenchang, P. Wenxiao, and Xu Mingyu, Int. J. Non-Linear Mech. **38**, 645 (2003).
[30] Martin Kroger, Phys. Rep. **390**, 453 (2004).
[31] Suchira Sen, Sanat K. Kumar, and Pawel Keblinski, Macromolecules **38**, 650 (2005).
[32] M. Kroger, W. Loose, and S. Hess, J. Rheol. **37**, 1057 (1993).
[33] M. Kroger and S. Hess, Phys. Rev. Lett. **85**, 1128 (2000).
[34] R. Yamamoto and A. Onuki, Phys. Rev. E **70**, 041801 (2004).
[35] J. Gao and J. H. Weiner, J. Chem. Phys. **103**, 1614 (1995).
[36] See, for example, Wolfram Mathworld, http://mathworld.wolfram.com/HeavisideStepFunction.html.